# Supporting information

## $CO_2$-driven fabrication of chiral fibers through amino acid self-assembly

Yu-di Zhu,[#a] Zi-You Pan,[#b] Zi-Ling Ye,[b] Chen-Cong Luo,[b] Rui Zhong,[a] Zheng-Luo Liu,[a] Anni Feng,*[a] Yang Yang*[b]

a. College of Chemical Engineering, Kunming University of Science and Technology, Kunming 650500, China.

b. Pen-Tung Sah Institute of Micro-Nano Science and Technology, State Key Laboratory of Physical Chemistry of Solid Surfaces, State Key Laboratory of Vaccines for Infectious Diseases, Xiang An Biomedicine Laboratory, Xiamen University, Xiamen 361005, China.

# Yu-di Zhu and Zi-You Pan contributed equally to this work.

## Contents

## Section 1. General information and instruments

Unless otherwise stated, all reagents were purchased from commercial suppliers and used directly without further purification. Routine $^{1}H$ NMR spectra (400 MHz) were recorded on a Bruker Avance II 400 MHz spectrometer at 298 K using tetramethylsilane (TMS) as an internal standard. Ultraviolet-visible (UV-Vis) absorption spectra were measured in quartz cuvettes using a JASCO V-780 spectrophotometer. Circular dichroism (CD) spectra were measured in a quartz cuvette on a JASCO J-1700 spectropolarimeter. High-resolution mass spectrometry (HRMS) data were obtained using an Agilent 6230 ESI-TOF MS spectrometer. Scanning electron microscopy (SEM) images were acquired on a ZEISS Sigma instrument operated at an accelerating voltage of 15 kV. Prior to SEM observation, the samples deposited on silicon wafers were sputter-coated with a thin platinum layer using a JEOL JFC-1600 auto fine coater to enhance conductivity.

Experimental details of CD testing: the optical path for all CD testing is 20 mm, and a self-made in-situ pressure testing apparatus was used, with quartz windows at both ends of the apparatus. Due to the increase in optical path and the fact that molecules hardly dissolve in water, to avoid signal distortion caused by excessive absorption, the absorbance was controlled at around 0.8, therefore, our sample concentration was 2 mg/mL. The CD testing was conducted at a scanning range of 300-200 nm, bandwidth of 1.0 nm, data interval of 1 nm, scanning speed of 200 nm/min, response time of 2 seconds, and 3 cumulative runs. Baseline correction was performed before the testing, and high-purity nitrogen gas was continuously blown through the optical path to remove the influence of oxygen during the testing.

Transmission electron microscopy (TEM) and energy-dispersive X-ray spectroscopy (EDS) analyses were performed on a JEM-F200 field-emission transmission electron microscope (JEOL, Japan) operated at an accelerating voltage of 200 kV. TEM images were acquired in bright-field mode. Elemental analysis and mapping were conducted using an energy-dispersive X-ray spectroscopy (EDS) detector equipped with a silicon drift detector (SDD) under scanning transmission

electron microscopy (STEM) mode.

For sample preparation, a drop of the dispersed sample suspension was deposited onto a carbon-coated copper grid and dried under ambient conditions prior to measurement.

## Section 2. Details of the synthesis of chiral nanofibers

### 2.1 Synthetic Scheme

Two enantiomeric pairs of amino acid-based amphiphiles were synthesized according to the reported method[1, 2]. Taking the synthesis of L-phenylglycine hexadecyl ester as an example: L-phenylglycine was dissolved in a mixed solvent consisting of 11 mL of 1 M aqueous sodium hydroxide solution, 11 mL of 10% aqueous sodium bicarbonate solution, and 10 mL of tetrahydrofuran (THF). At 0 °C, a solution of palmitoyl chloride (10 mmol, 3.00 mL) in 20 mL of THF was added dropwise to the reaction system, followed by continuous stirring for 3 hours. Upon completion, THF was removed under reduced pressure. The remaining aqueous solution was acidified with 2 M aqueous hydrochloric acid and then extracted with dichloromethane ($CH_2Cl_2$). The combined organic phases were dried over anhydrous sodium sulfate, and $CH_2Cl_2$ was removed by evaporation. The resulting solid was purified by silica gel column chromatography (eluent: petroleum ether/ethyl acetate = 10:1, v/v) and dried under vacuum to afford the target product with a yield of 55%.

D-Phenylglycine hexadecyl ester, L-phenylalanine hexadecyl ester, and D-phenylalanine hexadecyl ester were synthesized analogously, yielding 56%, 62%, and 67%, respectively. The structure and purity of all target molecules were confirmed by $^1$H NMR and HR-MS, ensuring their suitability for subsequent self-assembly studies.

### 2.2 Coating strategy of silica

To achieve the stabilization and functionalization of chiral fibrous structures, this study employs an in situ coating strategy to construct chiral silica composites[3]. Using compressed $CO_2$ as a green regulatory medium and without any organic additives, uniform coating of silica on the surface of self-assembled chiral fibrous structures of

amino acid amphiphiles was realized by controlling the hydrolysis-condensation process of the silica source, thereby effectively preserving their original morphology and chiral characteristics. Specifically, 0.25 mmol of the amphiphile was added to 15 mL of deionized water and dispersed by ultrasonication. The mixture was then transferred into a pressure vessel and stirred at 200 rpm. After sealing, $CO_2$ was introduced until the pressure stabilized at the desired value. The system was maintained at 25°C with continuous stirring for 1 h. Subsequently, 0.5 mL of tetraethyl orthosilicate (TEOS) was slowly injected into the solution to ensure homogeneous distribution of the silicon source. Under constant $CO_2$ pressure, the reaction proceeded for 12 h, allowing TEOS to gradually hydrolyze and condense in the weakly acidic environment formed by $CO_2$ and water, thereby generating a uniform silica layer both on the surface and within the fibrous matrix. After the reaction, the pressure was slowly released at a rate ≤ 0.2 MPa/min. The solid product was collected and alternately washed with deionized water and ethanol 3-5 times to remove unreacted TEOS, monomers, and byproducts. Finally, the sample was dried for subsequent SEM characterization.

**Section 3. ESI-MS characterization of amino acid amphiphiles**

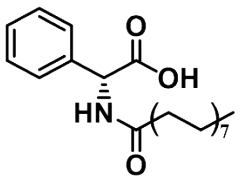


**Figure S1.** Line-drawing structure of M1 (L-Phg$C_{16}$)

HRMS (ESI)

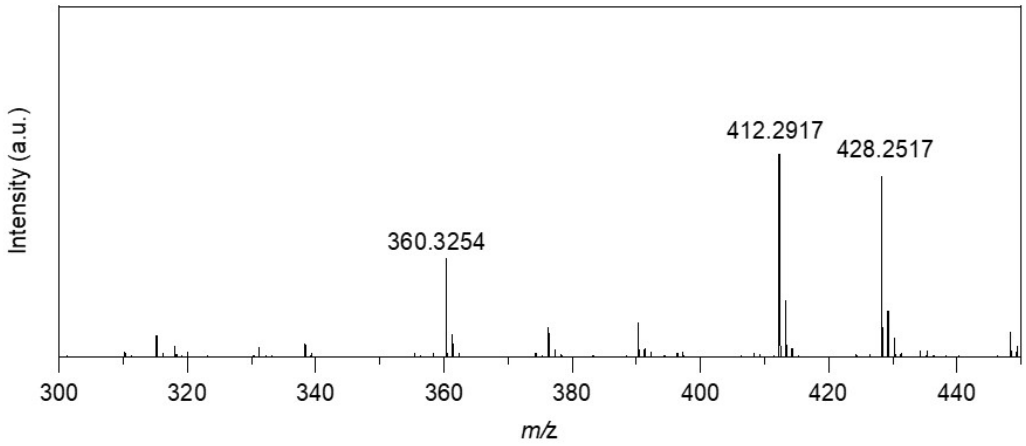


**Fig. S2** ESI-MS of M1 (L-PhgC$_{16}$). $[M+Na]^+$ calcd for $C_{24}H_{39}NO_3Na$: 412.2822, found, 412.2917.

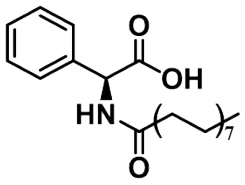


**Figure S3.** Line-drawing structure of M2 (D-PhgC$_{16}$)

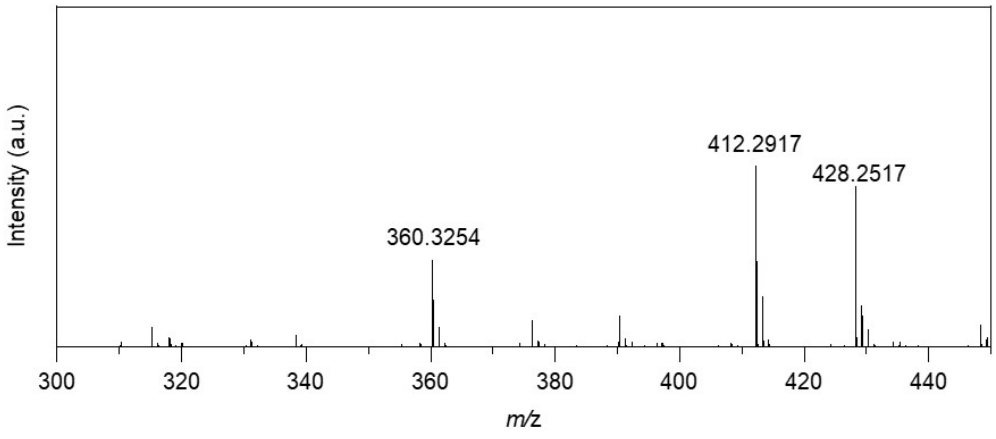


**Fig. S4** ESI-MS of M2 (D-PhgC$_{16}$). $[M+Na]^+$ calcd for $C_{24}H_{39}NO_3Na$: 412.2822, found, 412.2917.

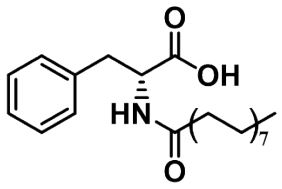


**Fig. S5** Line-drawing structure of M3 (L-PheC$_{16}$)

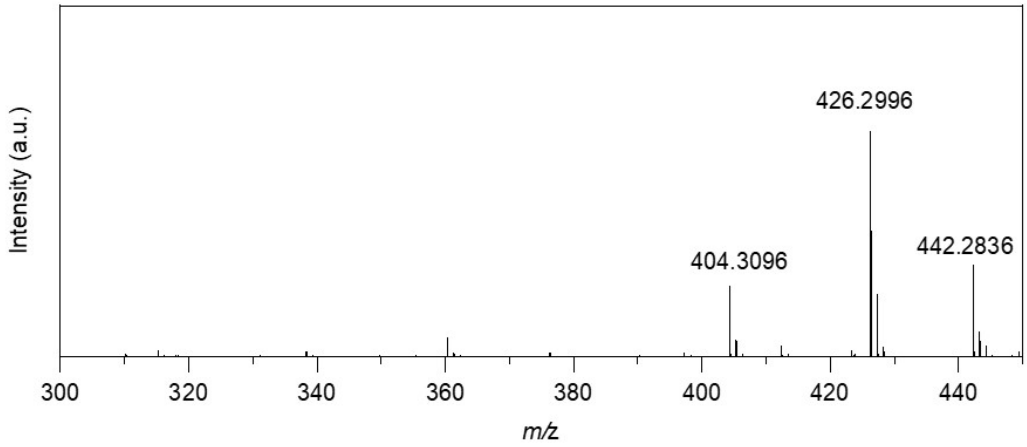


**Fig. S6** ESI-MS of M3 (L-PheC$_{16}$). $[M+Na]^+$ calcd for $C_{25}H_{41}NO_3Na$: 426.2979, found, 426.2996.

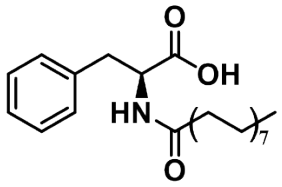


**Fig. S7** Line-drawing structure of M4 (D-PheC$_{16}$)

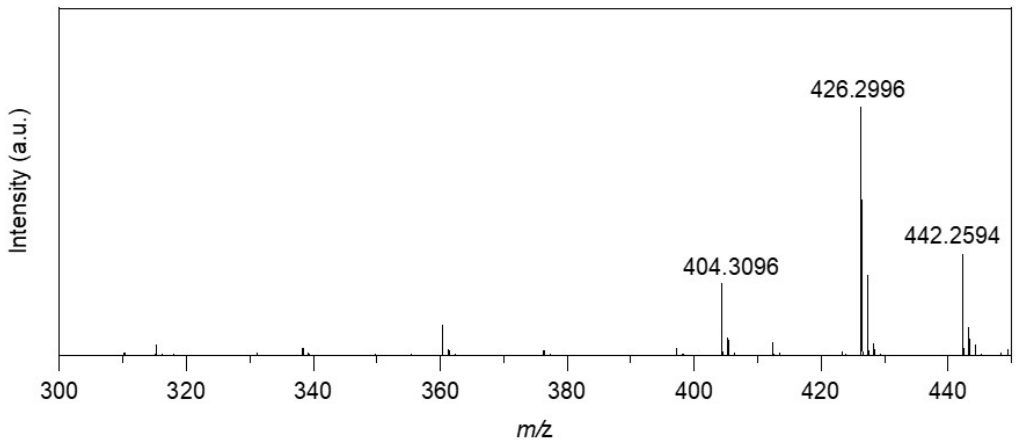


**Fig. S8** ESI-MS of M4 (D-Phe$C_{16}$). $[M+Na]^+$ calcd for $C_{25}H_{41}NO_3Na$: 426.2979, found, 426.2996.

## Section 4. SEM characterization

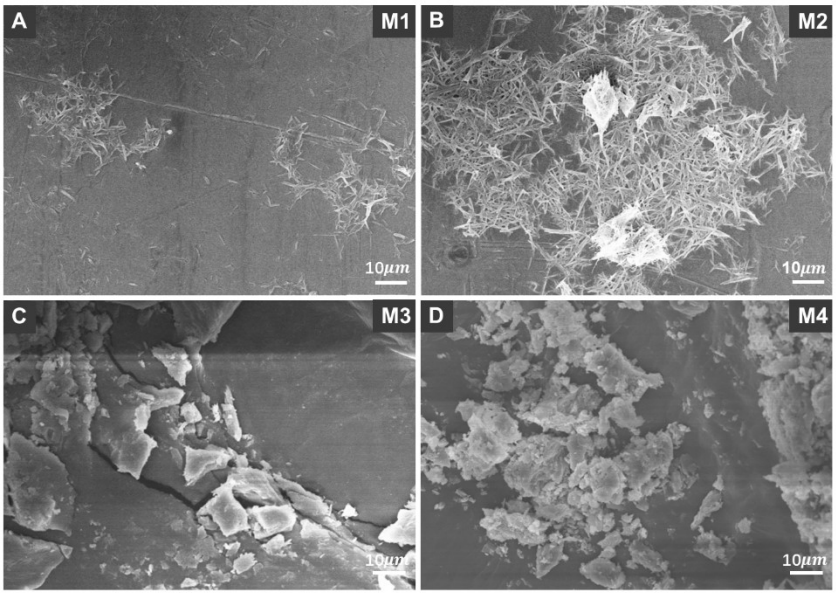


**Fig. S9** SEM images of molecule M1-M4 powders . A. M1. B. M2 C. M3 D. M4. All scale bars represent 10 μm.

To discuss the role of $CO_2$ during the fiber synthesis, we respectively conducted the reaction under 0 MPa $CO_2$ pressure and 0.15 mol/L TEOS for 12 h. As shown in the following **Fig. S10**, in the absence of $CO_2$, TEOS alone does not generate fiber

structures. There is just stainless steel substrate background can be seen in these images. This is because, without the acidic environment provided by the dissolved $CO_2$[4], TEOS cannot effectively undergo hydrolysis and therefore cannot form the silica structures. To further clarify the role of $CO_2$ in the self-assembly of amphiphilic molecules, we added 0.001 mol/L HCl solution to simulate the acidic environment in the absence of $CO_2$. **Fig. S11** gives the SEM images of products samples synthesized from M1-M4 under 0 MPa $CO_2$ pressure and 0.15 mol/L TEOS + 0.001 mol/L HCl after 12 h reaction time. It can be seen that there is no fiber structure but sheet-like silica structures formed under this condition. The above results demonstrated that $CO_2$ plays two important roles in the system. On one hand, it provides an acidic environment to facilitate the hydrolysis of TEOS. On the other hand, it promotes the self-assembly of amphiphilic molecules.

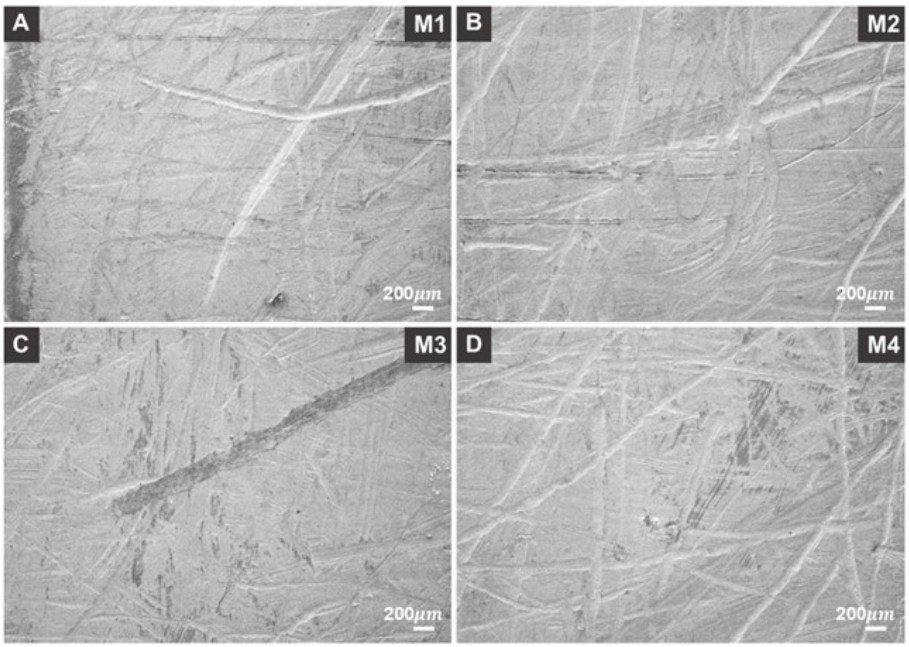


**Fig. S10** SEM images of products samples synthesized from M1-M4 under 0 MPa $CO_2$ pressure and TEOS of 0.15 mol/L after 12 h reaction time. A. M1. B. M2. C. M3. D. M4. All scale bars represent 200 μm. The substrates are stainless steel sheets.

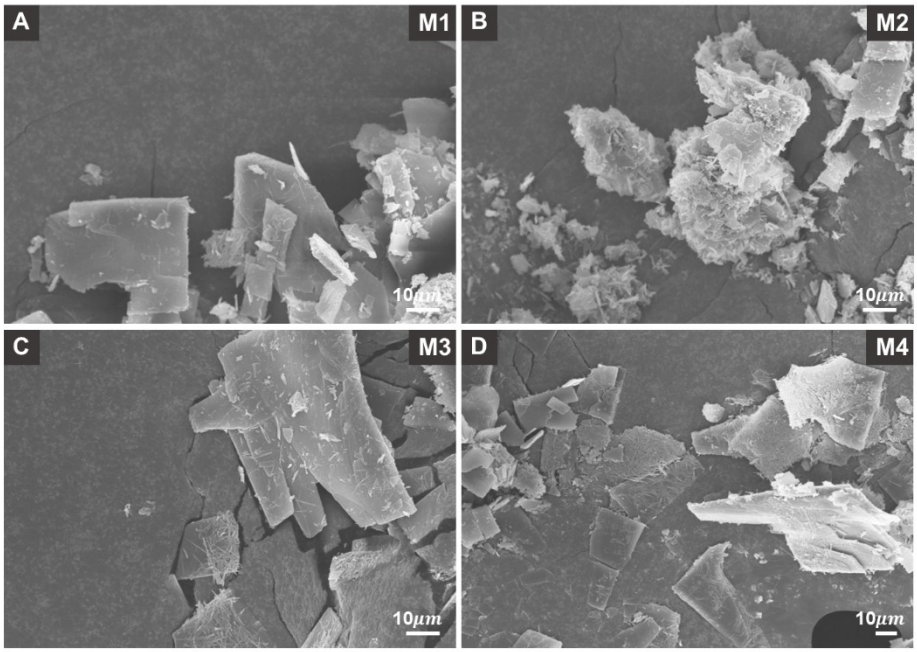


**Fig. S11** SEM images of products samples synthesized from M1-M4 under 0 MPa $CO_2$ pressure and 0.15 mol/L TEOS + 0.001 mol/L HCl after 12 h reaction time. A. M1. B. M2. C. M3. D. M4. All scale bars represent 10 μm.

To discuss the role of TEOS during the fiber synthesis, we investigated the effects of concentration of TEOS and reaction time. The following **Fig. S12** gives the SEM images of products samples synthesized from M1 under 3 MPa $CO_2$ pressure and TEOS of different concentrations after 12 h reaction time. It is found that when the TEOS concentration was 0.05 mol/L or 0.10 mol/L, no fiber structures were observed (**Fig. S12A and B**). This may be attributed to insufficient hydrolysis and condensation at low TEOS concentrations, thus is unfavorable for the deposition of silica on/among the amphiphilic blocks and then preventing the formation of stable and observable fiber structures. When the TEOS concentration was increased to 0.15 mol/L, distinct fibrous structure can be observed (**Fig. S12C**). Therefore, 0.15 mol/L was selected as the appropriate TEOS concentration in this work. Besides, we investigated the effect of reaction time on the synthesis of fibers. The following **Fig. S13** gives the SEM images of products samples synthesized from M1 under 3 MPa $CO_2$ pressure and 0.15 mol/L TEOS with different reaction time. It can be seen that when the reaction is 6 h and 8 h (**Fig. S13A and B**), no visible fiber product was observed. When the reaction time

increased to10 h (**Fig. S13C**), similar fiber structures began to appear, but the production was extremely low and the repeatability was poor. When the reaction time was extended to 12 h, the fiber structures could be stably observed. Therefore, 12 h was selected as the reaction time in this work.

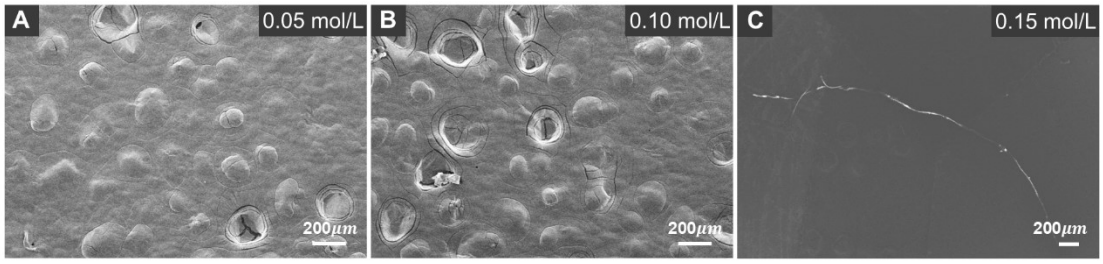


**Fig. S12** SEM images of products samples synthesized from M1 under 3 MPa $CO_2$ pressure and TEOS of different concentrations after 12 h reaction time. A. TEOS of 0.05 mol/L. B. TEOS of 0.10 mol/L. C. TEOS of 0.15 mol/L. All scale bars represent 200 μm.

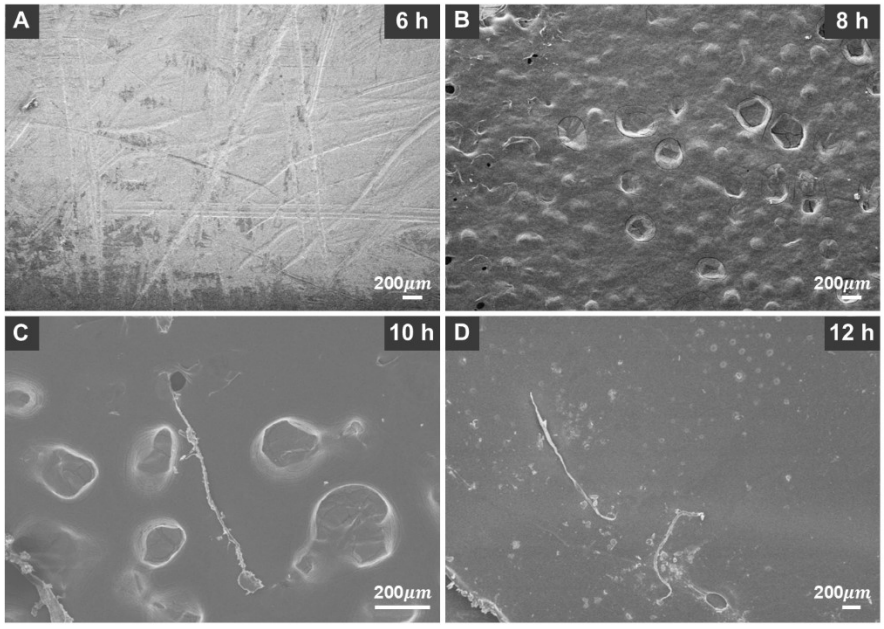


**Fig. S13** SEM images of products samples synthesized from M1 under 3 MPa $CO_2$ pressure and 0.15 mol/L TEOS with different reaction time. A. 6 h. B. 8 h. C. 10 h. C. 12 h. All scale bars represent 200 μm.

It was found that fibers structure cannot be formed without silica coating (Figs. S14-S17).

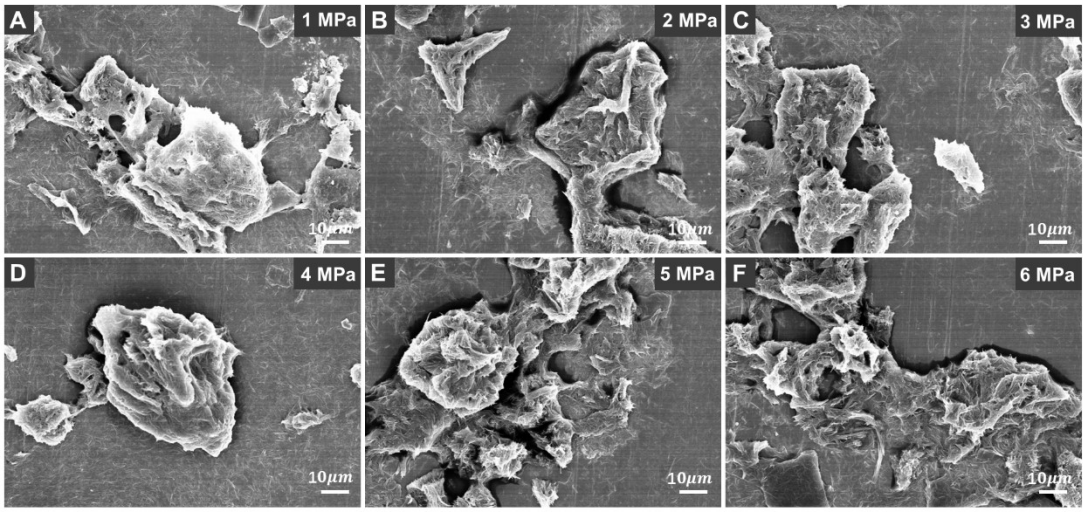


**Fig. S14** SEM images of Fib1 without silica coating under different $CO_2$ pressures. A.1 MPa. B. 2 MPa. C. 3 MPa. D.4 MPa. E. 5 MPa. F.6 MPa. All scale bars are 10 μm.

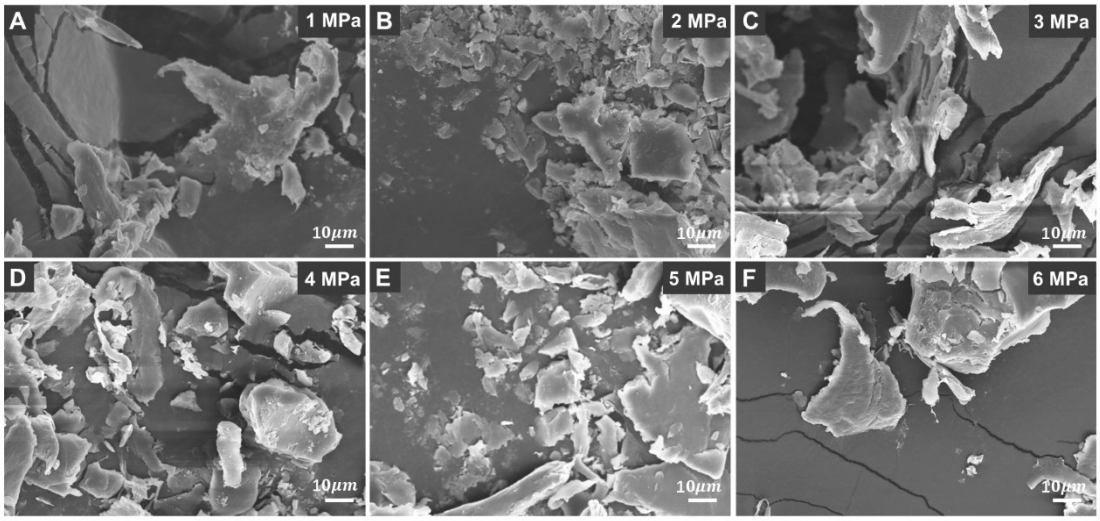


**Fig. S15** SEM images of Fib2 without silica coating under different $CO_2$ pressures. A.1 MPa. B. 2 MPa. C. 3 MPa. D.4 MPa. E. 5 MPa. F.6 MPa. All scale bars are 10 μm.

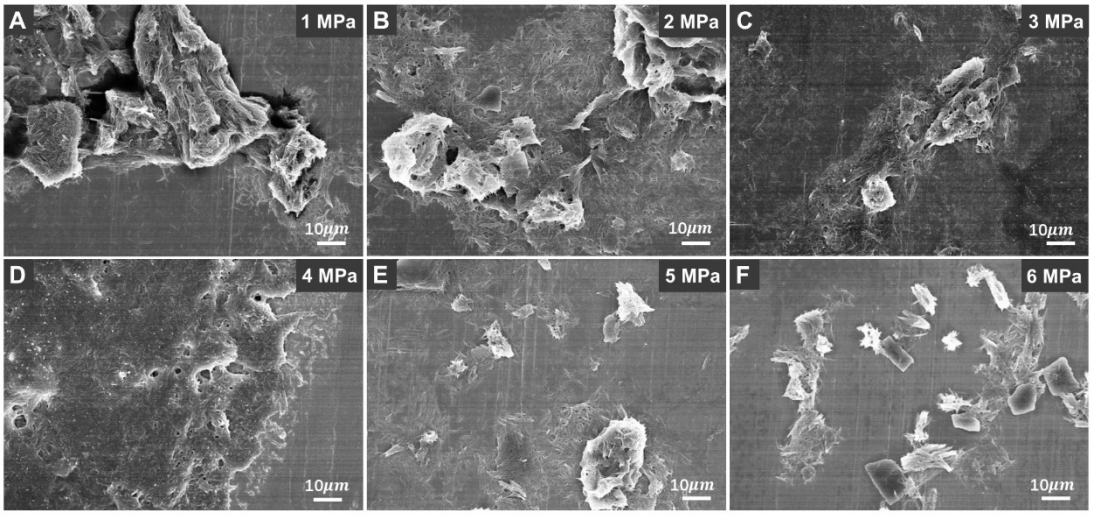


**Fig. S16** SEM images of Fib3 without silica coating under different $CO_2$ pressures. A.1 MPa. B. 2 MPa. C. 3 MPa. D.4 MPa. E. 5 MPa. F.6 MPa. All scale bars are 10 μm.

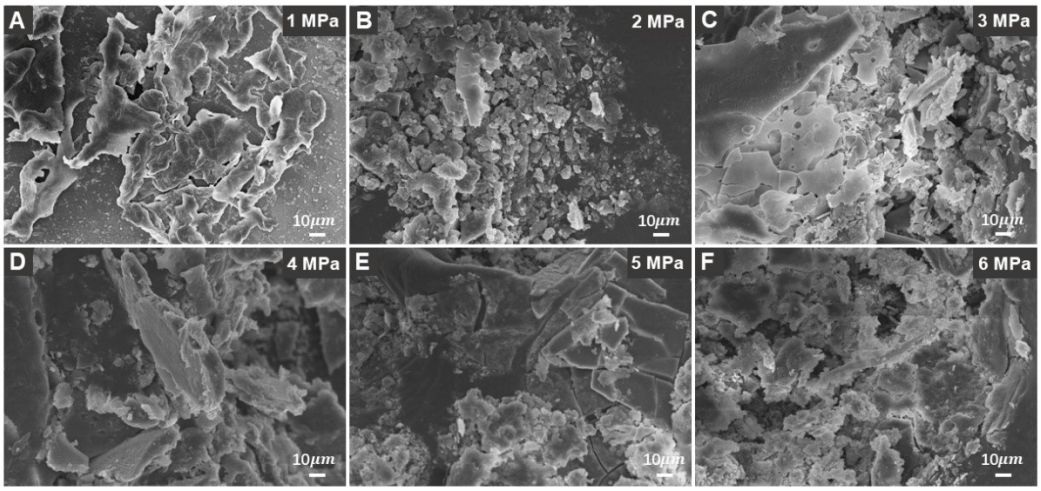


**Fig. S17** SEM images of Fib4 without silica coating under different $CO_2$ pressures. A.1 MPa. B. 2 MPa. C. 3 MPa. D.4 MPa. E. 5 MPa. F.6 MPa. All scale bars are 10 μm.

Fig. S18 gives SEM image of product synthesized under the TEOS of 0.15 mol/L and different $CO_2$ pressures without amphiphilic molecules. It can be seen that there is no fiber structure formed, which demonstrated that the main structure of the fibers is formed by the assembly of amphiphilic molecules, while $SiO_2$ mainly plays a role in stabilizing the morphology.

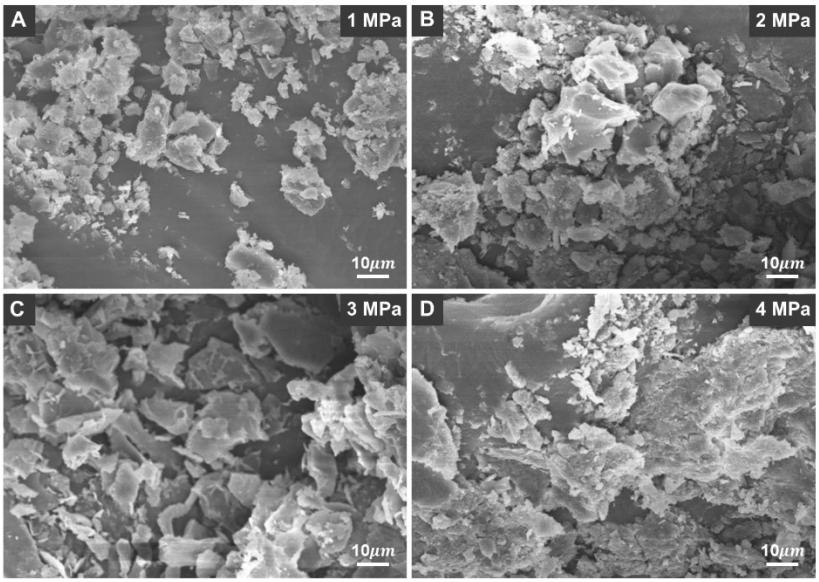


**Fig. S18** SEM image of product synthesized under the TEOS of 0.15 mol/L and different $CO_2$ pressures without amphiphilic molecules. A. 1 MPa. B 2 MPa. C. 3 MPa. D. 4 MPa. All scale bars are 10 μm.

In contrast, after silica coating, the fibers exhibit a uniform structure with good dispersibility, regular morphology, and no obvious aggregation (Figs. S19–S22). These results indicate that silica coating can effectively fix the morphology of the fibers, thereby addressing the issues of structural instability and aggregation tendency in the uncoated system.

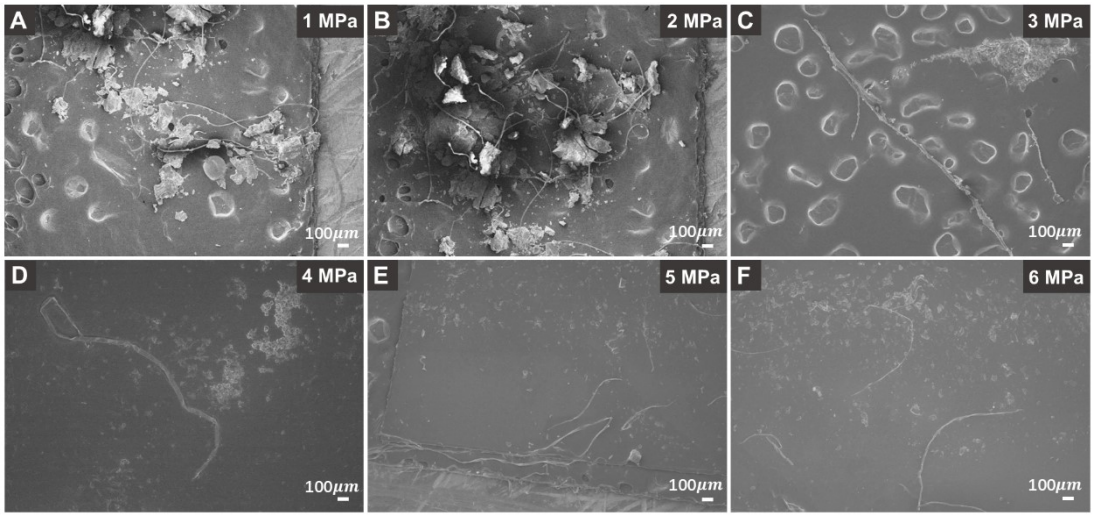


**Fig. S19** SEM images of Fib1 after silica coating under different $CO_2$ pressures. A.1 MPa. B. 2 MPa. C. 3 MPa. D.4 MPa. E. 5 MPa. F.6 MPa. All scale bars are 100 μm.

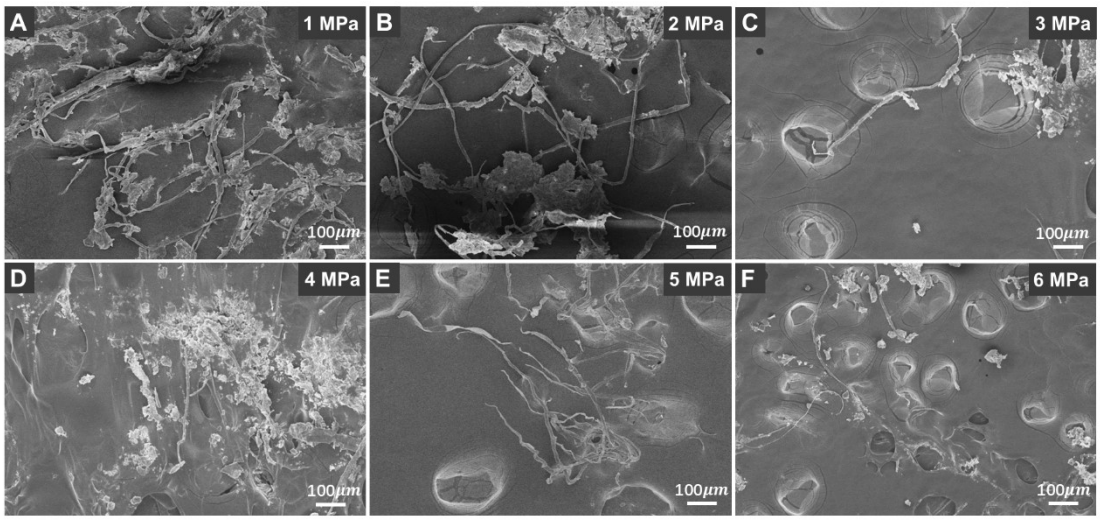


**Fig. S20** SEM images of Fib2 after silica coating under different $CO_2$ pressures. A.1 MPa. B. 2 MPa. C. 3 MPa. D.4 MPa. E. 5 MPa. F.6 MPa. All scale bars are 100 μm.

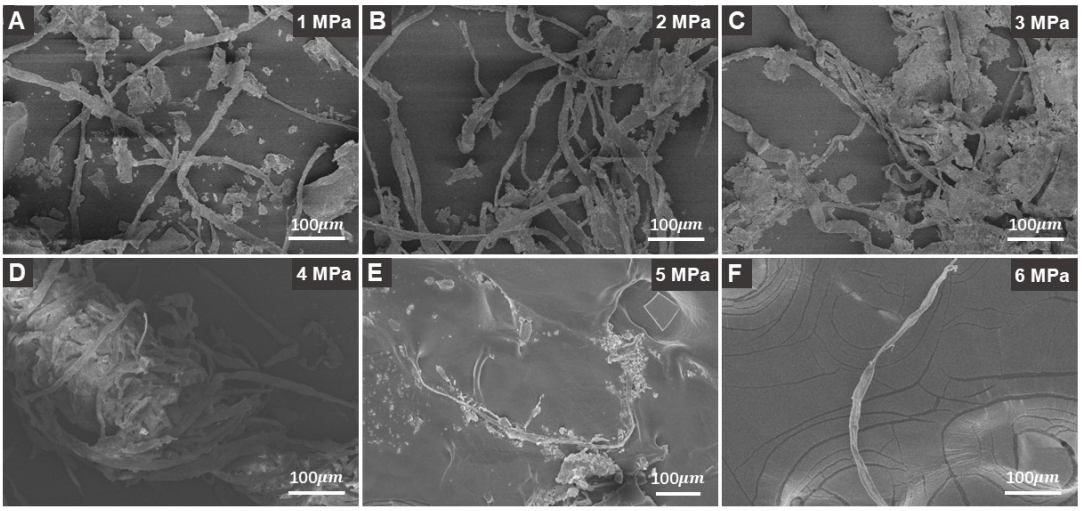


**Fig. S21** SEM images of Fib3 after silica coating under different $CO_2$ pressures. A.1 MPa. B. 2 MPa. C. 3 MPa. D.4 MPa. E. 5 MPa. F.6 MPa. All scale bars are 100 μm.

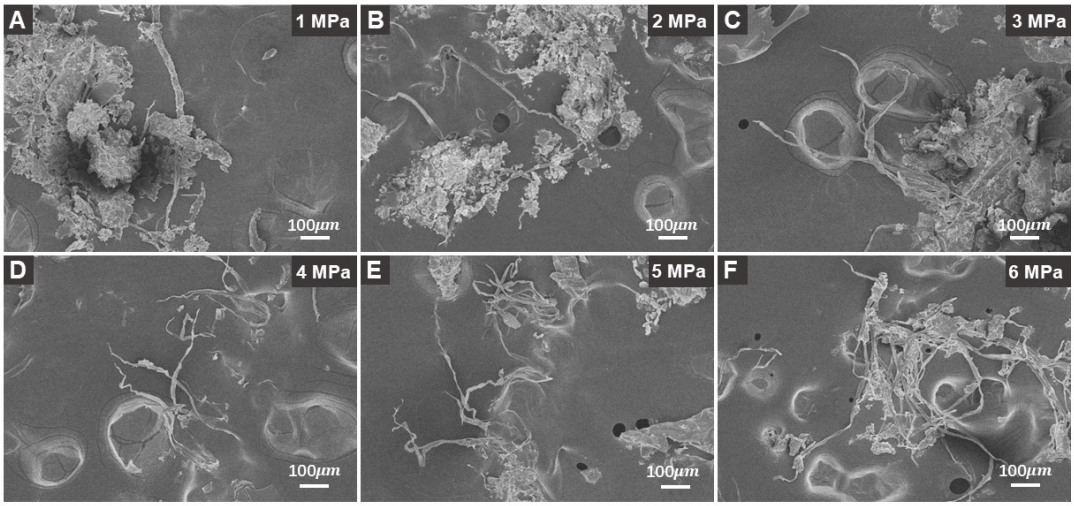


**Fig. S22** SEM images of Fib4 after silica coating under different $CO_2$ pressures. A.1 MPa. B. 2 MPa. C. 3 MPa. D.4 MPa. E. 5 MPa. F.6 MPa. All scale bars are 100 μm.

We performed additional TEM, TEM-EDX, and TGA to further investigate the internal structure and overall composition of the fibers.

First, in order to preserve as much of the organic component in the sample as possible, the as-prepared microwire samples were directly subjected to TEM-EDX analysis without ethanol washing. As shown in the following **Fig. S23**, there is a relatively strong carbon signal (**Fig. S23B**), indicating the presence of carbon-containing/organic-related components in the fibers. We speculate that this carbon signal may arise from both retained organic molecules and partially hydrolyzed or condensed TEOS-related species. This result confirms the existence of organic components in the sample.

To further examine the possible presence of the organic core, we subsequently washed the microwire samples with ethanol to reduce the influence of residual species and then carried out TEM-EDX analysis as shown in the following **Fig. S24**. The TEM results revealed a distinct inner core region that can be differentiated from the outer silica layer in the cross-sectional area, supporting the existence of an organic core in the fiber structure. However, under the current TEM sample preparation and characterization conditions, we were unable to directly observe a clear core–shell

interface or a silica-free organic core. We speculate that this may be related to the limited mechanical stability of the sample. Since TEM characterization generally requires smaller and/or thinner structural units, the silica-coated fibers, being relatively fragile, may undergo fracture or delamination during sample preparation, dispersion, or electron-beam exposure. Nevertheless, the TEM images show that the exfoliated silica layers are relatively thin, which to some extent suggests that the sample is not a fully dense and homogeneous silica solid.

In addition, thermogravimetric analysis (TGA) was conducted to evaluate the overall content of organic components in the fibers. The TGA results, as shown in the following **Fig. S25**, also indicated that a certain proportion of organic matter is indeed present in the samples, with contents of 4.90 wt% (Fib1), 5.10 wt% (Fib2), 5.00 wt% (Fib3), and 6.10 wt% (Fib4), respectively. These findings further demonstrate that, in addition to silica, the fibers contain a non-negligible amount of organic components.

Furthermore, we conduct the reaction under the TEOS of 0.15 mol/L and different $CO_2$ pressures without amphiphilic molecules. As shown in the following Fig. S18, there is no fiber structure formed, which demonstrated that the main structure of the fibers is formed by the assembly of amphiphilic molecules, while $SiO_2$ mainly plays a role in stabilizing the morphology.

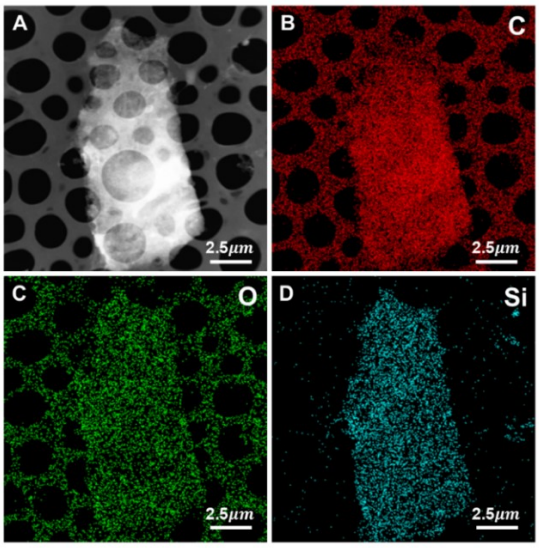


**Fig. S23** TEM-EDS analysis of unwashed Fib1. A. TEM image of Fib1. B. e EDS mapping of carbon. C. EDS mapping of oxygen. D. EDS mapping of silicon. All scale

bars are 2.5 μm.

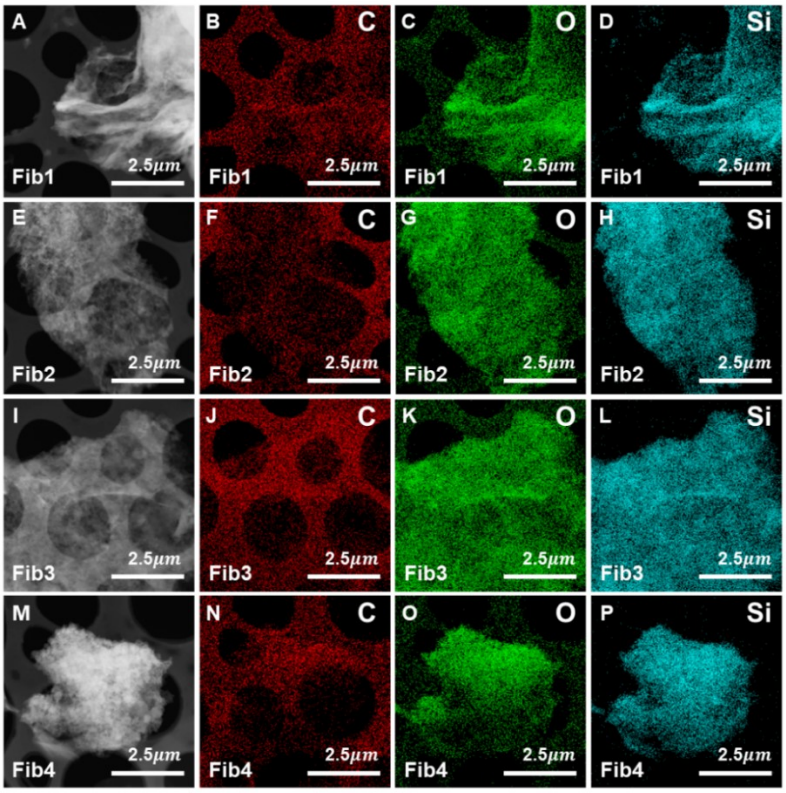


**Fig. S24** TEM-EDS analysis of ethanol washed Fib1-Fib4. A-D. TEM image and EDS mapping of Fib1. E-H. TEM image and EDS mapping of Fib2. I-L. TEM image and EDS mapping of Fib3. M-P. TEM image and EDS mapping of Fib4. All scale bars are 2.5 μm.

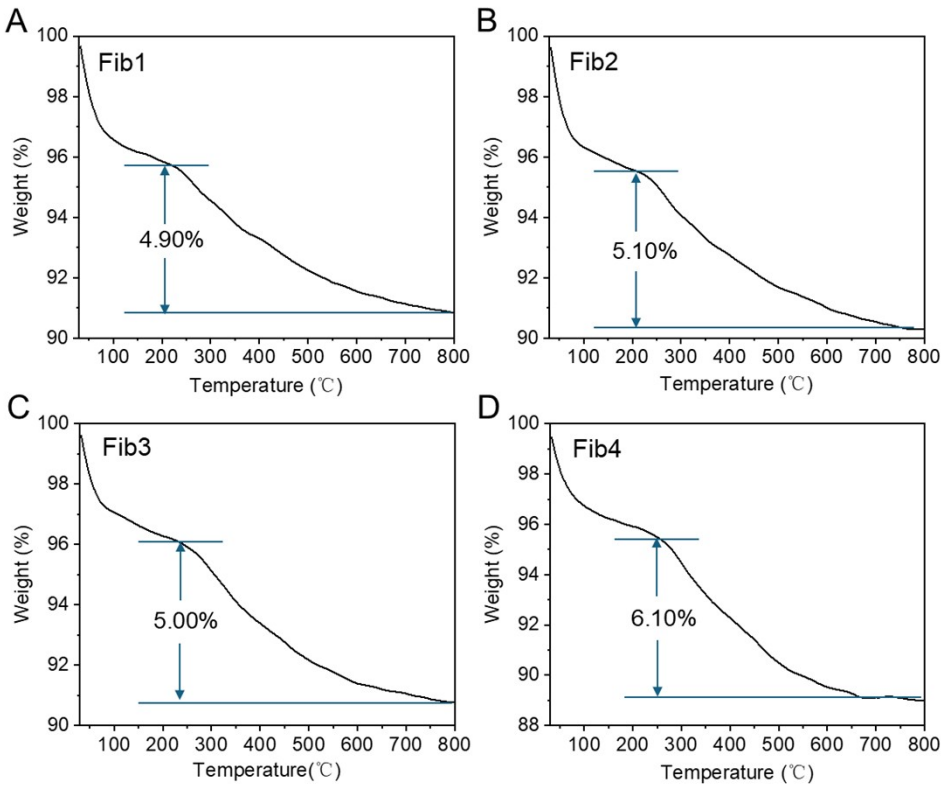


**Fig. S25** Thermogravimetric analysis of Fib4-Fib4. A. Fib1. B. Fib2. C. Fib3. D. Fib4.

## Section 5. CD characterizationi

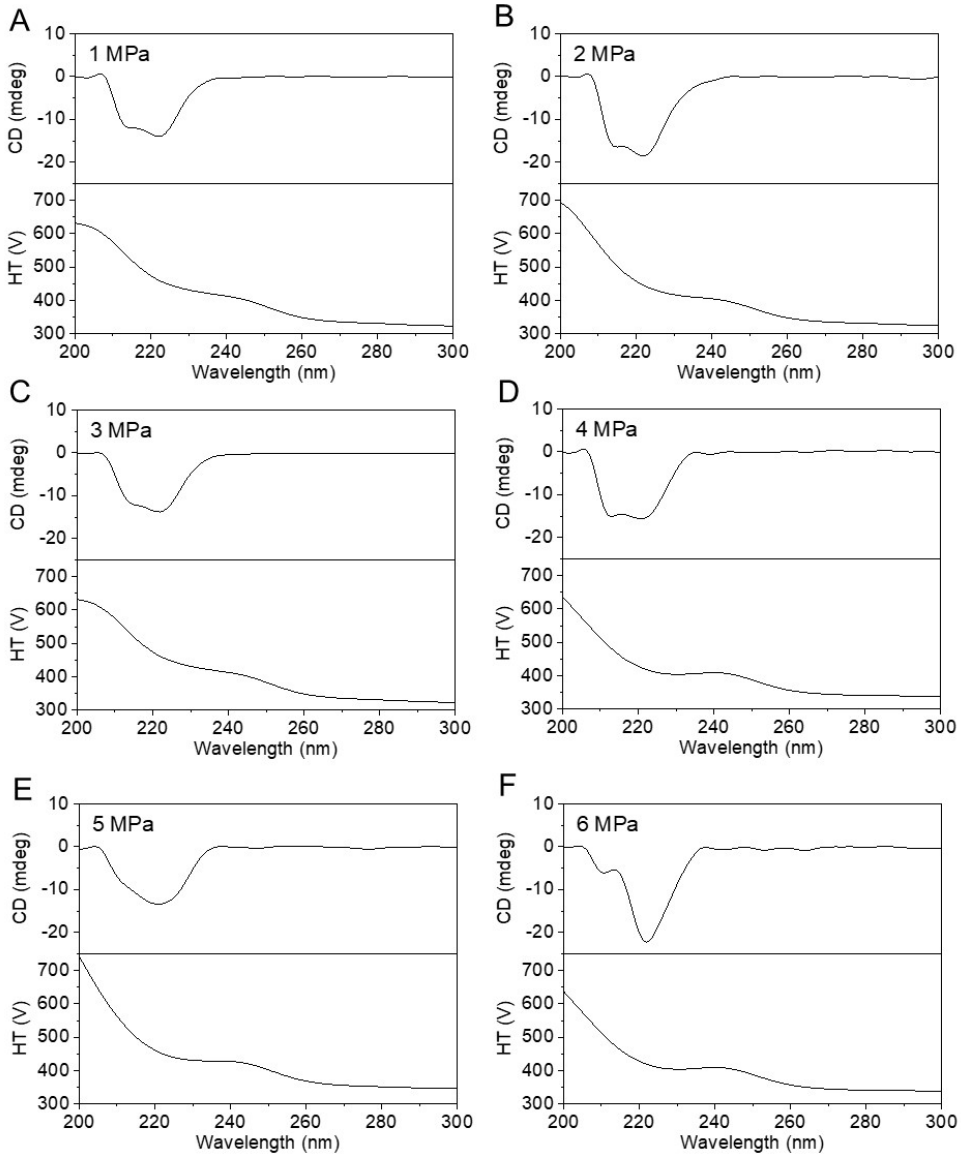


**Fig. S26** Plot of CD absorbance and photomultiplier voltage over wavelength for Fib1 under $CO_2$ pressure from 1 MPa to 6 MPa.

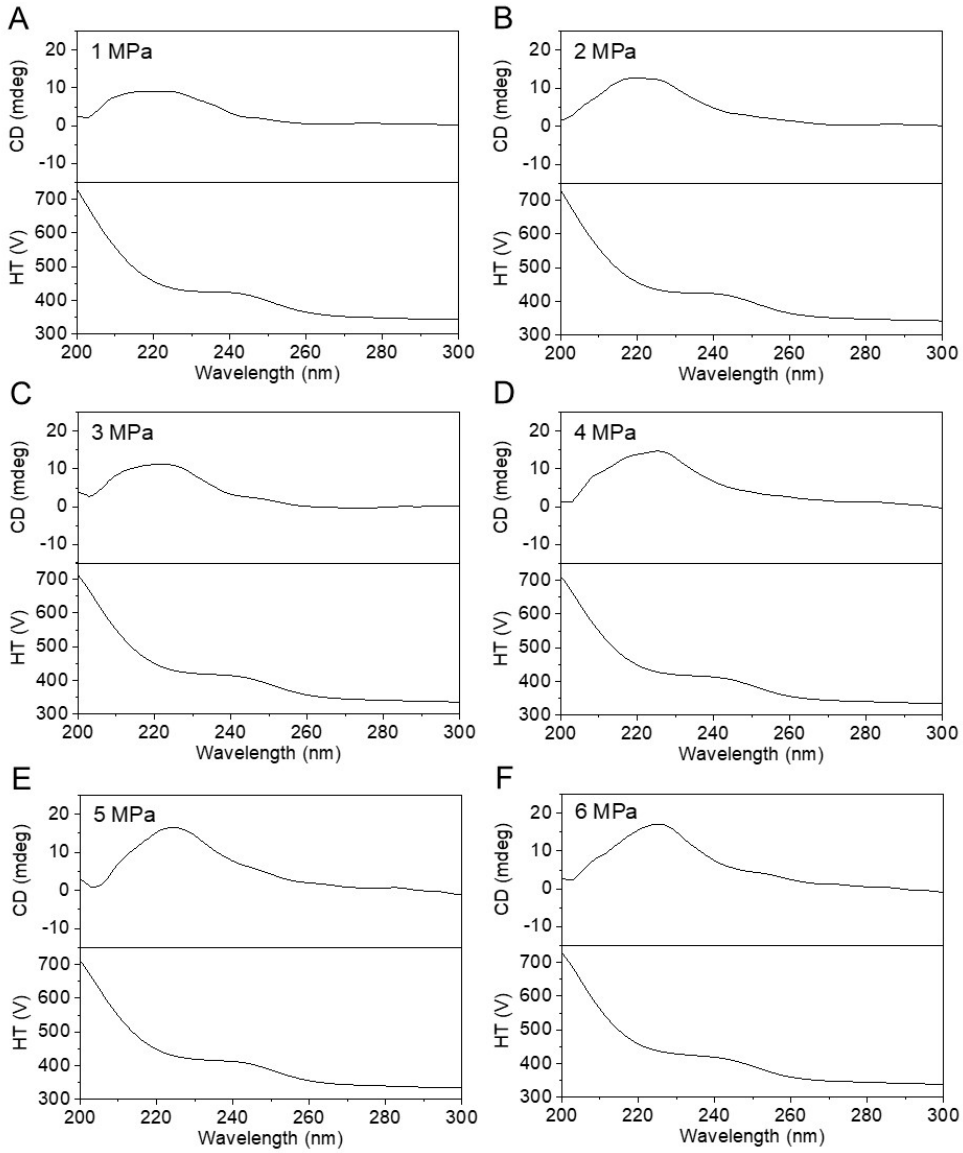


**Fig. S27** Plot of CD absorbance and photomultiplier voltage over wavelength for Fib2 under $CO_2$ pressure from 1 MPa to 6 MPa.

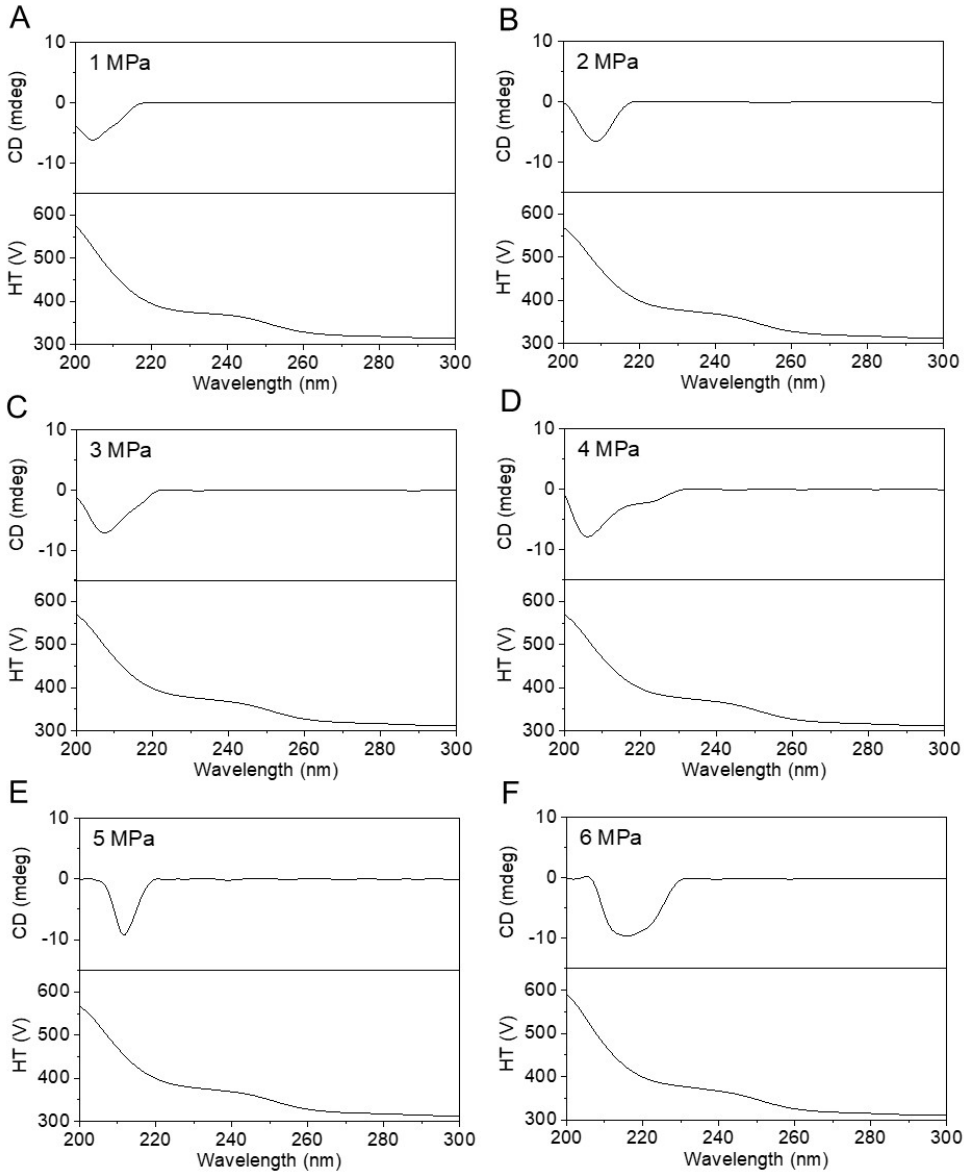


**Fig. S28** Plot of CD absorbance and photomultiplier voltage over wavelength for Fib3 under $CO_2$ pressure from 1 MPa to 6 MPa.

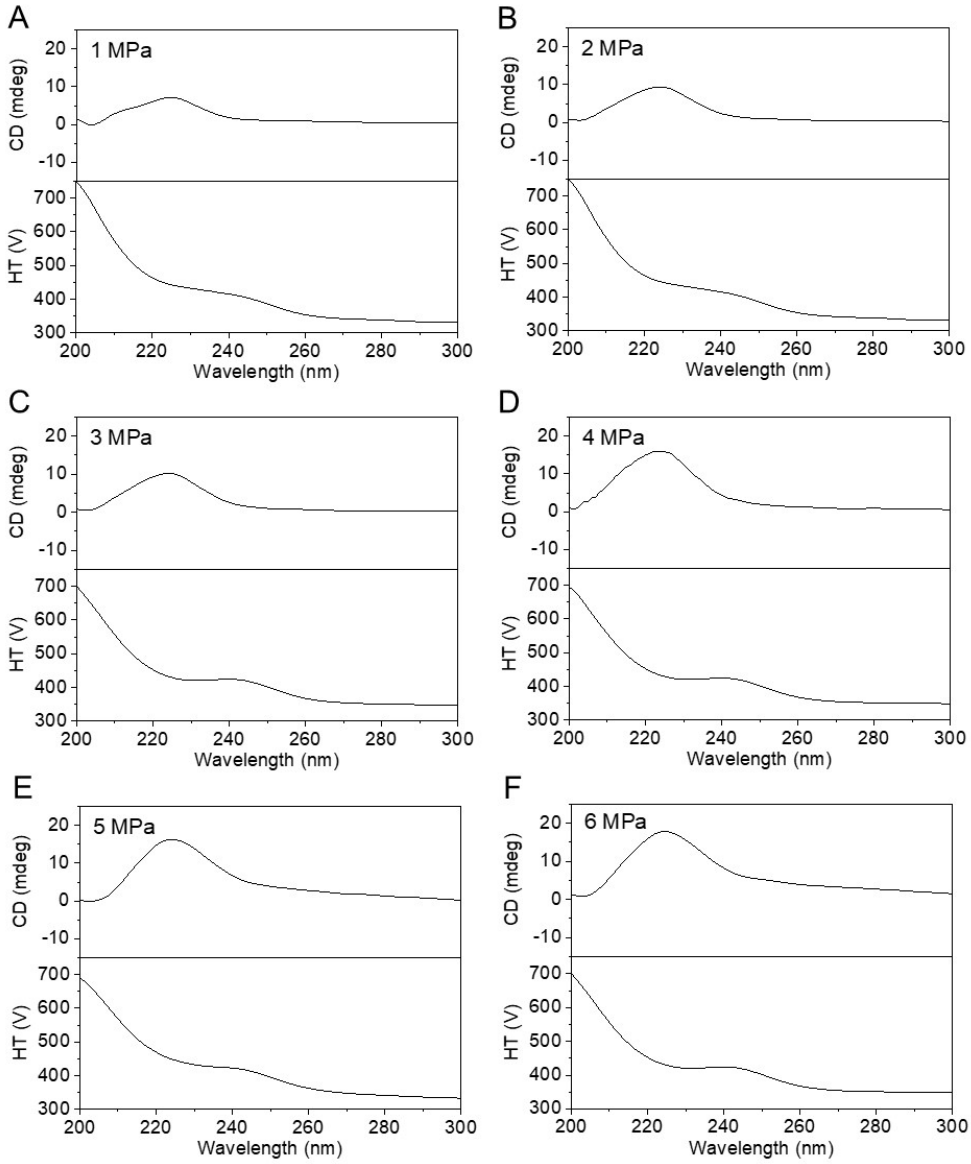


**Fig. S29** Plot of CD absorbance and photomultiplier voltage over wavelength for Fib4 under $CO_2$ pressure from 1 MPa to 6 MPa.

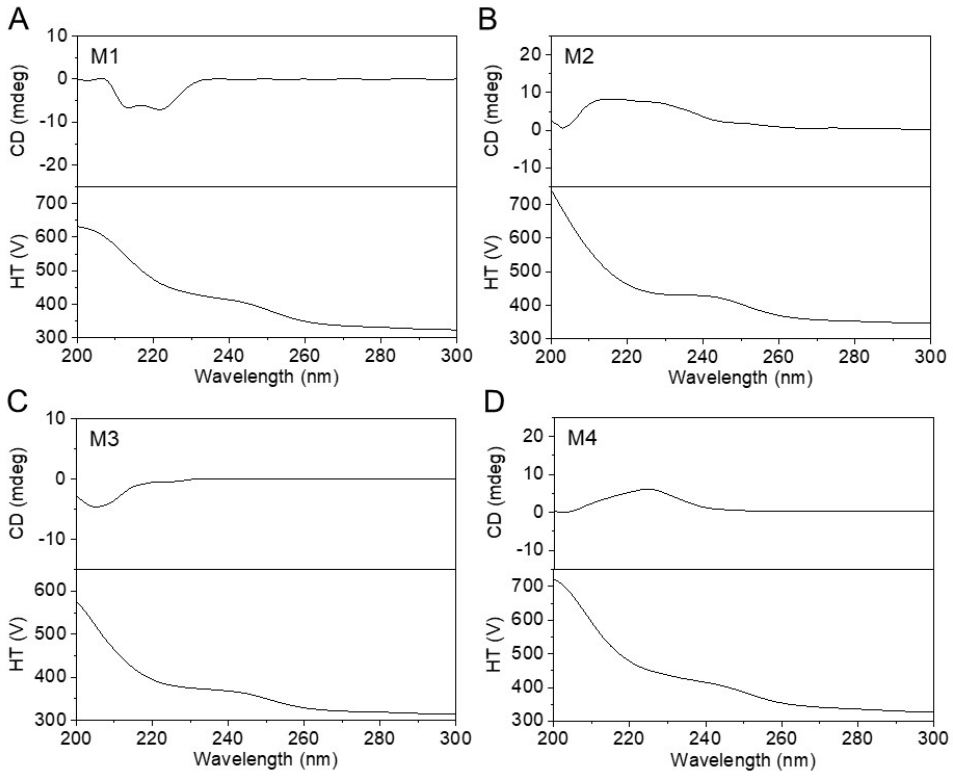


**Fig. S30** Plot of CD absorbance and photomultiplier voltage over wavelength for M1-M4 dissolved in water.

## References


1. M. Gerova, F. Rodrigues, J.-F. Lamère, A. Dobrev and S. Fery-Forgues, *J. Colloid Interface Sci.*, 2008, **319**, 526-533.
2. C. Gao, S. Li, C. Zhao, Q. Sun, X. Sun, L. Ge, L. Wang, Z. Xi, J. Han and R. Guo, *Small*, 2024, **20**, 2310234.
3. W. Li, J. Zhang, S. Cheng, B. Han, C. Zhang, X. Feng and Y. Zhao, *Langmuir*, 2009, **25**, 196-202.
4. K. L. Toews, R. M. Shroll, C. M. Wai and N. G. Smart, *Anal. Chem.*, 1995, **67**, 4040-4043.